STATISTICAL STUDIES OF THE RELATIONSHIP BETWEEN THE AMPLITUDE OF POSITIVE MAGNETIC BAYS AT MID-LATITUDES, GEOMAGNETIC ACTIVITY AND PARAMETERS OF THE SOLAR WIND

©2025 A.A. Lyubchich [1*], I.V. Despirak [1], R. Werner [2***]**

[1] *Polar Geophysical Institute, Apatity (Murmansk region), Russia*

[2] *Space Research and Technology Institute at the Bulgarian Academy of Sciences, Stara Zagora, Bulgaria*

[*] *e-mail: lubchich@pgia.ru*

[**] *e-mail: despirak@gmail.com*

[***] *e-mail: rolwer52@yahoo.co.uk*

Received March, 03 2024

Revised June, 23 2024

Accepted for publication July, 25 2024

Abstract. During the expansion phase of the substorm, the poleward jump of the aurora (breakup) and the expansion of the auroral bulge are observed. The expansion is accompanied by a negative magnetic bay under the aurora and a positive magnetic bay at the middle latitudes. The amplitude of the negative bay is characterized by the auroral AL index. To characterize the positive bay, the MPB index (Mid-latitude Positive Bay index) was previously proposed. The paper examines the statistical relationship of the MPB index with the geomagnetic activity at different latitudes and with the parameters of the solar wind and the interplanetary magnetic field. It is shown that all extremely large values of the MPB index (above 10,000 nT^2) are observed during strong geomagnetic storms (when the Dst index drops below –100 nT), and all extremely strong geomagnetic storms (when the Dst index drops below –250 nT) accompanied by extremely high MPB index values. Statistically, the MPB index increases with the increasing of geomagnetic activity at any latitudes. The MPB index, on average, increases with the increasing of the magnitude of the interplanetary magnetic field and any of its components. But for the Bz component, large values of the MPB index are observed by its southward direction. For plasma parameters of the solar wind, the MPB index increases most strongly with the increasing of the solar wind speed. There is also the strong dependence on the dynamic pressure and on the magnitude of the E_Y component of the solar wind electric field. However, the MPB index weakly depends on solar wind density and temperature.

Keywords: *geomagnetic indices, magnetic storms, solar wind, interplanetary magnetic field, statistical analysis*

DOI: 10.31857/S00167940250106e2

1. INTRODUCTION

The poleward leap of auroras (breakup) and the expansion of the auroral bulge are important signs of a magnetospheric substorm. The expansion of the auroral bulge is accompanied by the development of negative magnetic bays at auroral latitudes and positive magnetic bays at middle latitudes. The appearance of magnetic bays is caused by the development of the substorm current wedge, which occurs due to partial destruction of the cross-tail (dawn-dusk) current in the near tail of the magnetosphere, for example, due to the reconnection of geomagnetic field lines. As a result, a large-scale three-dimensional current system is formed, in which the section of the destroyed magnetospheric tail current is redirected along the geomagnetic field lines to the ionosphere, closed at auroral latitudes by the westward electrojet, and returns to the magnetosphere in the evening sector as a field-aligned current created by precipitating accelerated electrons. Very intense substorms, during which the *SML* -index of geomagnetic activity drops below –2500 nT, are often classified separately as supersubstorms [Tsurutani et al., 2015; Hajra et al., 2016, etc.]. During supersubstorms, an additional current wedge of the opposite direction can form on the evening side (for example, [Fu et al., 2021; Zong et al., 2021; Despirak et al., 2022]).

Mid-latitude positive magnetic bay in the *X* -component of the magnetic field at stations in the near-midnight sector, associated with the development of the substorm current wedge, consists of a short phase of growth, lasting about 20 minutes, and usually a slightly slower phase of decline. At a fixed moment in time, the spatial distribution of positive variations in the *X* -component represents a Gaussian profile, symmetrical relative to the center of the current wedge. The spatial variation in the *Y* -component resembles one cycle of a sinusoidal wave with a maximum in the evening sector, at the longitude of the outflowing current, and a minimum in the morning sector, at the longitude of the inflowing current (details are shown, for example, in Fig. 9 from McPherron et al. [1973]). Thus, the position of the extremes of the northern and eastern components of the magnetic field can be used to characterize the substorm current wedge.

Using this circumstance, for the analysis of manifestations of substorm activity at middle latitudes, a new one-minute geomagnetic *MPB* -index (*Mid-latitude Positive Bay index*) was recently introduced in 2015. The methodology for its calculation is described in detail in [Chu, 2015; McPherron and Chu, 2017, 2018]. The index characterizes the power of disturbances in the horizontal component of the magnetic field at mid-latitude stations during the development of the substorm current wedge. It is determined by the sum of squares of disturbances in the northern and eastern components of the magnetic field.

The authors of the index (McPherron and Chu) proposed two methodologies for calculation that differ in details, which led to the creation of two similar, but still slightly different, sets of values *MPB* -index. A description of the differences in calculation methods can be found, for example, in the work by McPherron and Chu [2017]. One of the differences is that the first set (let's call it the McPherron list) was obtained from data from 35 stations with geomagnetic latitude λ_{mag} between –45 ° and 45 ° , while the second set (Chu list) was compiled from data from 41 stations in the Northern and Southern hemispheres with $20° < |\lambda_{mag}| < 52°$. The first list can be found in the supplementary information to the online version of the article by McPherron and Chu [2018]. It includes one-minute values of the total power of horizontal magnetic field variations, that is $\Delta X^2 + \Delta Y^2$, for the period from February 1980 to the end of 2012 (until the end of 1984, the data are episodic, irregular). The Chu list, at the time of its presentation, separately included one-minute variations ΔX^2 (let's denote them as *MPB* X *X*), ΔY^2 (*MPB* Y *Y*), as well as their sum from the beginning of 1991 to the end of 2019. We will use this one in our work. Therefore, let's briefly describe the algorithm for obtaining the *MPB* -index according to Chu's methodology. First, secular variations and solar-diurnal *Sq variations* are removed from the original magnetic field measurement data from 41 stations. The former are removed using a linear trend, the latter using the epoch superposition method for 21 days. Then the remaining low-frequency variations are removed using a high-pass filter with a cutoff frequency at 12 hours. Further, only data from stations located in the night sector at the given moment, ±5 hours from 23.5 hours local time, are kept. These data are squared and averaged across all "night" stations. As a result, the values *MPB* X *X* and *MPB* Y *Y* are obtained. Their sum gives the total *MPB* -index at the given moment of time.

Sometimes it is of interest to analyze variations of the magnetic field at a specific magnetic station at middle latitudes. This possibility is described in [Werner et al., 2021] , where an improved methodology for calculating the *MPB* -index was proposed. In particular, data from the Bulgarian station Panagyurishte (Panagjurishte (PAG), 42.5° N, 24.2° E; $\lambda_{mag} \approx 37°$) were taken into account.

It should be noted that sometimes variations of not the *MPB* -index itself, but its square root are analyzed (for example, [Sergeev et al., 2020; Tsyganenko et al., 2021]).

The paper presents a statistical analysis of the *MPB* -index, as well as an investigation of its relationship with both geomagnetic activity at different latitudes and with solar wind (SW) parameters and the interplanetary magnetic field (IMF).

2. DATA

For the analysis, one-minute values of the *MPB* -index for the period from 1991 to 2019 were taken. For the same period, one-minute values of other geomagnetic indices characterizing magnetic activity at different latitudes were taken. Let's list them, moving from the pole to the equator.

– To characterize disturbances in the northern polar cap, we will use the *PC* (*N*)-index [Troshichev and Andrezen, 1985; Troshichev et al., 1988; Troshichev, 2010]. Index values are available in the OMNI database on the website (https://cdaweb.gsfc.nasa.gov/). As is known, the *PC* -index is calculated from data from one station located near the geomagnetic pole. In the Northern hemisphere, for the *PC* (*N*) index, this is the Qaanaaq (Thule) (THL) station, 77.5 ° N 290.8 ° E; λ mag $_{\text{mag}} \approx 86.7°$), in the southern hemisphere, for *PC* (*S*), it is the Vostok station. The *PC* -index is proportional to the geoeffective interplanetary electric field and is an indicator of the amount of energy entering the Earth's magnetosphere [Troshichev and Andrezen, 1985; Troshichev et al., 1988; Troshichev, 2010].

– Disturbances in the auroral zone are characterized by indices of the *AE* (*AE* , *AL* , *AO* , *AU*) family, determined from data of 12 auroral stations. The indices *AL* and *AU* are defined by the maximum negative and positive deviation of the *H* -component of the geomagnetic field from the quiet level for these stations and depend on the intensity of the westward and eastward auroral electrojet currents. The *AE* index determines the total range of deviations of the *H* -component of the geomagnetic field, that is, it equals the sum of the absolute values of *AL and* и*AU indices.* indices.*AO* -index equals half the sum of *AL and* и*AU indices.* The indices are available on the website (https://wdc.kugi.kyoto-u.ac.jp/aeasy/index.html).

– The indices *SML* and *SMU* are determined similarly to *AL* and *AU* indices, but using data from all magnetic stations of the SuperMAG project with geomagnetic latitudes from +40 to +80 ° . The indices are available on the website (http://supermag.jhuapl.edu/indices/). They better describe processes in the auroral oval under highly disturbed conditions, for example, during magnetic storms, when the auroral oval can significantly deviate toward the equator from its position under quiet conditions. With such deviations, the stations used in calculating indices of the *AE* family may end up outside the auroral oval area; as a result, the *AE* -index will cease to reflect the intensity of electrojets [Feldstein, 1992].

– Indices *ASY* H *H* , *ASY* D *D* and *SYM* H *H* , *SYM* D *D* are available on the website (https://wdc.kugi.kyoto-u.ac.jp/aeasy/index.html). The calculation procedure and analysis of indices, for example, for 1992, one of the first years analyzed in this work, are described in detail in [Iyemori et al., 1994]. Data from nine geomagnetic stations located at middle and low latitudes are used,

including three stations used to calculate the *Dst* -index. Monthly, the indices are calculated using six stations out of nine, and the selection of six stations may vary from month to month. *SYM* H *H* is essentially the averaged deviation of the *H* -component of the geomagnetic field from the quiet level at selected stations with a correction for their geomagnetic latitudes, similar to the procedure for calculating the *Dst* -index. *SYM* D *D* is calculated from the averaged deviations of the *D* -component of the geomagnetic field, but without correction for station latitudes. The indices *SYM* H *H* and *SYM* D *D* characterize the longitude-symmetric part of the ring current. The indices *ASY* H *H* and *ASY* D *D* determine the range between the maximum and minimum values of *H and иD* -components of the geomagnetic field at six stations after subtracting the corresponding symmetric parts from the disturbance field and, thus, characterize the longitude-asymmetric part of the ring current. We will classify *ASY* H *H* and *ASY* D *D* as mid-latitude indices since their calculation includes data from mid-latitude stations. Wanliss and Showalter [2006] concluded that, generally, the *SYM* H *H* index differs little from the low-latitude *Dst* -index, and it can be used as a *Dst* -index with high (one-minute) resolution. Based on this, we will classify *SYM* H *H* and *SYM* D *D* as low-latitude indices.

– Hourly average values *Dst* -index – from the website (https://wdc.kugi.kyoto-u.ac.jp/dst_final/index.html).

One-minute values of the IMF magnitude B_T and its components *Bx* , *By* , *Bz* (in *GSE* and *GSM* coordinate systems) and solar wind data (velocity magnitude and its components, density, temperature, dynamic pressure, as well as the E_Y-component of the electric field and the ratio of plasma pressure to magnetic pressure β) were taken from the OMNI database from the website (https://cdaweb.gsfc.nasa.gov/).

3. RESULTS

3.1. Cases of extremely large MPB-index values

Most increases in the *MPB* -index are associated with substorm activity. The criterion for determining the substorm onset time based on *MPB* -index variations is when the peak value of the *MPB* -index exceeds 25 nT^2 [McPherron and Chu, 2017, 2018]. But sometimes the *MPB* -index reaches very large values. We selected all cases where the *MPB* X *X* exceeded 10 000 nT^2 (that is, when the ΔX variation exceeded 100 nT).

Fig. 1.

An example of such an event is presented in Fig. 1, which shows the values of the magnitude and two components of the IMF, several solar wind parameters, and geomagnetic indices for 24

hours starting from 12:00 UT on 06.04.2000. It can be seen that the *MPB* -index exceeds 10 000 nT^2 (this value is shown on the graph by a dotted line), reaching ~60 000 nT^2 during the main phase of the magnetic storm with $Dst_{min} = -288$ nT. Magnetic storms are often divided into groups based on the Dst_{min} value. Strong (*intense*) magnetic storms are conventionally defined as those with $Dst_{min} < -100$ nT [for example, Gonzalez and Tsurutani, 1987]. Tsurutani et al. [1992] considered five very intense (*great*) magnetic storms with Dst_{min} from –249 nT and below. Mac-Mahon and Gonzalez [1997] called such very intense magnetic storms superstorms, using the criterion $Dst_{min} < -240$ nT. Later, in the works [Gonzalez et al., 1999, 2002], the numerical criterion for very intense magnetic storms was refined: $Dst_{min} < -250$ nT. We will use this refined criterion in the future. According to this criterion, the extremely high values of the *MPB* -index, shown in Fig. 1, were observed during a superstorm. Fig. 1 shows that the differences between the *SYM* H *H* and *Dst* indices, if we do not take into account their different time resolutions, are insignificant, which justifies classifying *SYM* H *H* as a low-latitude index. It is also visible that during the main phase of the storm, the difference between the *SML* and *AL* indices can indeed be significant; the indices can differ in magnitude by a factor of two or more.

Superstorms are a rare phenomenon, from 1957 to 2018, only 39 events were recorded, the list of which is provided in the work [Meng et al., 2019], of which only 14 have been observed since 1991, when data on the magnitude of the *MPB* -index is available in the Chu list we use. Analysis showed that during all 14 events, extremely large values of the *MPB* -index were observed. This can be seen from Table 1, in which superstorms registered since 1991 are ranked by the minimum value of the *Dst* -index. The first five columns are taken from Table 1 in the article by Meng et al. [2019]. The last column shows the magnitude and time of registration of the extreme value of the *MPB* -index.

Table 1.

It should be noted that during two storms – 08.11.2004 and 06.11.2001 – *MPB* X *X* was below the specified threshold value, nevertheless the full *MPB* -index exceeded 10 000 nT^2.

As a rule, the maximum values of the *MPB* -index were registered close to the moment of the *Dst* minimum, the average time difference between these events was ~3 h. But in the last two superstorms (10.11.2004 and 29.10.1991), the moment of the maximum of the *MPB* -index was closer to the moment of observation of the sudden impulse SI$^+$.

The remaining events with extremely large values of *MPB* -index (*MPB* X $X > 10\ 000$ nT^2) occurred during strong magnetic storms ($Dst_{min} < -100$ nT). The corresponding results are shown in Table 2. Since the *Dst* -index has an hourly resolution, the time in the second column is a multiple of

30 minutes – the middle of the hour or, for the storm of 02.06.1992, the middle of a two-hour interval with the minimum value of the *Dst* -index. The first storm in the table with $Dst_{min} = -247$ nT is sometimes also classified as a superstorm (for example, [Gonzalez et al., 2011]). In most cases, extreme values of the *MPB* -index were observed near the moment when the minimum value of the *SYM* H *H* index was recorded.

Table 2.

Note that nine more superstorms were recorded from 1980 to 1990, when data on the *MPB* -index from the first list [McPherron and Chu, 2018] are available. During all these superstorms, abnormally high values of the *MPB* -index (> 10 000 nT^2) were also recorded.

3.2. Statistical relationship of the MPB-index with geomagnetic indices

All one-minute data on the *MPB* -index were taken for the entire analyzed interval from 1991 to 2019, while no additional analysis was conducted on whether the observed variations were accompanied by substorm development or not.

Fig. 2.

The distribution of the *MPB* -index by values is shown in Fig. 2. The tail of the distribution in a double logarithmic scale is well approximated by a straight line with a negative slope of ~ –2.3 (wide gray line on the graph), i.e., it has a power-law form: $N \approx b \times MPB^{-2.3}$. The graph is constructed with a step of 1 nT *MPB* -index values, which also describes well the region of small index values, up to the substorm threshold value of 25 nT^2 for the^2. The graph with a step of 100 nT^2, describing the region above the threshold value, is given in [Lyubchich et al., 2023]. It is well described by a power law across the entire range of values with a close power exponent: –2.5.

Such power-law distribution can be considered as a special case of the Pareto distribution (for example, [Arnold, 2015]). Power-law distributions decay slower than exponential ones, which is why they are often used to analyze the distribution of extreme values. For example, [Tsubouchi and Omura, 2007] used the Pareto distribution to analyze the probability of strong magnetic storms. They showed that the distribution of storms by intensity becomes power-law at $Dst < -280$ nT. This threshold value is close to the superstorm criterion, which confirms the statistical validity of introducing this separate class of storms. [Nakamura et al., 2015] used the Pareto distribution to analyze the distribution of *AL-, „AU- and AE* - indices and concluded that there should be limit values for the indices: $AL \sim -4200$ nT and $AU \sim 2000$ nT, meaning that the current in the western and eastern electrojets should have a limit value. They analyzed the period from 1996 to 2012. In our work, the interval 1991−2019 is considered. The lowest value of the *AL* -index during our

interval turned out to be –4141 nT and occurred during the main phase of the most powerful magnetic storm (20.11.2003, Dst_{min} = –422 nT).

An example of another type of distributions used, among other things, in extreme value theory, is the Weibull distribution [Weibull, 1951; Coles, 2001]. Werner et al. [2023] showed that the distribution of the number of events with a positive bay at middle latitudes depending on the local *AL* -index, determined by selected stations of the IMAGE magnetometer network (*International Monitor for Auroral Geomagnetic Effects*) *(IL* -index –IMAGE *electrojet Lower index*), is well described by the Weibull distribution. In particular, the recurrence of events with specified extreme values of the *IL* -index was estimated.

We analyzed the statistical relationship *of the MPB* -index with other one-minute geomagnetic indices. For this purpose, regression lines of the *MPB* -index were constructed relative to the indices mentioned in Section 2. The dependence of any value *Y* on the value *X* is manifested in the change of mean values of *Y* when *X* changes. To determine this dependence, the array *X* was divided into uniform segments X_i, and for each segment, the mean value Y_i was calculated. Similarly, the dependence of *X* on *Y* can be determined. As is known, if there is no direct functional relationship, then the dependencies $Y(X)$ and $X(Y)$ will not coincide.

Fig. 3.

The relationship of the *MPB* -index with the *SML* index is shown in Fig. 3. Fig. 3 *a* shows the distribution of the *SML* index by values. Similar to Fig. 2, the graph is plotted on a double logarithmic scale, so the absolute value of *SML* was taken. The tail of the distribution in the double logarithmic scale is approximated by a straight line with a slope of ~ –5.2 (wide gray band on the graph). As can be seen from Fig. 3 *b* , the *MPB* -index monotonically increases with the increase in auroral activity, which is indicated by the *SML* index. The dependence of *MPB* on the absolute value of *SML* is close to a power law – the approximation is shown in Fig. 3 *b* for values of *SML* < –300 nT, with a power exponent of ~2.3. The inverse dependence, shown in Fig. 3 *c* , has a different form: the *SML* -index first decreases (increases in absolute value) with the growth of *MPB* , then, when *MPB* reaches ~ 4000 nT^2, it approaches a horizontal asymptote of approximately –1100 nT (horizontal segment on the graph).

Fig. 4.

Fig. 4 demonstrates the statistical dependence *of the MRV* -index on geomagnetic indices that characterize disturbances in the polar cap (Fig. 4 *a* , $PC(N)$-index), at middle (Fig. 4 *b* , index *ASY* H *H*) and low (Fig. 4 *c* , index *SYM* H *H*) latitudes. The *MRV* -index depends more strongly on positive values of the $PC(N)$-index, monotonically increasing with their growth. At $PC(N) > 2$,

the increase is close to a power law with an exponent slightly above two (2.35) (shown by the gray band on the right part of Fig. 4 *a*). As known, the positive *PC* (*N*)-index characterizes the impact of geoeffective interplanetary electric field; substorms and magnetic storms begin when the *PC* -index exceeds the threshold value of ~2 mV/m [Troshichev, 2010]. And negative values of the *PC* -index are associated with the impact of the northern component of the IMF on the magnetosphere. In this region, the growth of the *MRV* -index is close to exponential (gray wide line in the left part of Fig. 4 *a* , for *PC* (*N*) < 0. The *MRV* -index monotonically increases with the growth of the *ASY* H *H* index, and at *ASY* H *H* > 20 nT, the dependence is a power law (shown by the gray line in Fig. 4 *b*), with the exponent being the same as for *PC* (*N*) > 2. The *MRV* -index also monotonically increases with the growth of the absolute value of the *SYM* H *H* index, depending more strongly on its negative values. At *SYM* H *H* < –50 nT, the growth follows a power law, quadratic, that is $|SYM - H| \sim \sqrt{MPB}$. For positive values, the growth of the *MRV* -index is close to exponential. Both dependencies are shown by gray lines in Fig. 4 *c* .

3.3. Correlation of MPB-index with Solar Wind and Interplanetary Magnetic Field Parameters

For analysis, we will use minute data from the OMNI database: IMF magnitude and the magnitude of its components in two Cartesian coordinate systems – *GSE* and *GSM* , the magnitude and direction of SW velocity, its density, temperature and dynamic pressure, as well as the geoeffective component of the electric field and the parameter β , which is the ratio of plasma thermal pressure to magnetic pressure.

Fig. 5.

The dependence of the *MPB* -index on the characteristics of the interplanetary magnetic field is shown in Fig. 5. As can be seen from Fig. 5 *a* , the *MPB* -index monotonically increases with the growth of the IMF modulus B_T, approaching extreme values at very large values of B_T. The regression line for the *By component* of the IMF weakly depends on the sign of the component, i.e., the graph is almost symmetrical relative to the zero value of *By* (Fig. 5 *b*). The *MPB* -index increases with an increase in the modulus of the *Bz component* of the IMF (Fig. 5 *c*), but it is much higher at negative values of *Bz* – for example, *MPB* is about 10 times greater at *Bz* = –30 nT than at *Bz* = +30 nT. Figure 5 is constructed in the *GSM* coordinate system. The corresponding dependencies for the IMF components in the *GSE* system are given in [Lyubchich et al., 2023].

The most influential plasma parameters of the solar wind on the *MPB index* are its velocity *V* (and the radial component V_x), as well as the dynamic pressure P_{dyn}. The dependence of the *MPB* -index on $V_x$is close to exponential (the approximation is shown in Fig. 6 *a* by a gray line). When the

velocity changes four times, from 250 to 1000 km/s, the *MPB* -index changes from almost zero to ~2 000 nT ^{2}. The dependence of the *MPB* -index on the solar wind dynamic pressure for values of $P_{dyn} \leq 40$ nPa is close to power-law, with an exponent of 1.3 (gray line in Fig. 6 *b*). *MPB* -index changes approximately within the same limits as in Fig. 6 *a*). *MPB* -index increases almost linearly with the growth of solar wind density, but the range of index changes is relatively small - from ~30 to ~300 nT ^{2}, therefore the dependence of the *MPB* -index on the SW density can be considered weak . Due to this, at very high values of the SW dynamic pressure ($P_{dyn} > 40$ nPa), usually observed at high density and not very high solar wind speed, the dependence of the *MPB-index* on P_{dyn} reaches saturation (*MPB* ~ 2000 nT ^{2}) or even begins a slight decrease in the *MPB* -index values with further growth of the solar wind dynamic pressure. However, this result is statistically unreliable due to the small number of such extreme events. At SW temperature up to 10 000 K we have *MPB* ≈ 40 nT ^{2}, then the *MPB* value decreases by almost half, reaching its minimum value at *T* ≈ 14 000 K, and then begins to monotonically, almost linearly, increase, reaching 700 nT ^{2} at a temperature of one million degrees Kelvin. *MPB* -index strongly depends on the geoeffective component of the solar wind electric field ($E_{Y GSM}$). The dependence of the *MPB* -index on $E_{Y GSM}$ (Fig. 6 *c*) is similar to the dependence of the *PC* (*N*)-index (Fig. 4 *a*). By analogy with Fig. 4 *a* in the left part of Fig. 6 *c* , for $E_{Y GSM}$ from –15 mV/m to 0, an exponential approximation is shown, and in the right part, for $E_{Y GSM}$ from 2 to 30 mV/m – a power law. *MPB* -index practically does not depend on the plasma β .

Fig. 6.

4. DISCUSSION

In section *3.1* . it was shown that all cases of extremely large values of the *MPB* -index occurred during the development of strong (–250 nT < $Dst_{min} \leq$ –100 nT) and very strong ($Dst_{min} \leq$ –250 nT) magnetic storms (superstorms). During magnetic storms, the auroral oval expands and shifts towards the equator. At this time, the middle latitudes, where the magnetic stations used to calculate the *MPB* -index are located, become auroral or close to them in their properties, which explains the discovered dependency.

During the two strong magnetic storms listed in Table 2 (01.10.2002 and 26.02.1992), even the minimum one-minute values of the *SYM* H *H* index turned out to be greater than the hourly average value of Dst_{min}. It can be assumed that this is due to differences in the list of stations used, in

the methodology for determining baselines, and so on. Comparison of *Dst* and *SYM* H *H* indices is conducted, for example, in [Wanliss and Showalter, 2006].

The correlation *3.2* . found in section *MPB* -index, introduced for the analysis of substorm activity manifestations at middle latitudes, with the increase in deviation from the quiet level of other geomagnetic indices can be explained as follows. The size of the auroral oval depends on magnetic activity. Under quiet conditions, it resembles a ring with a width of ~2°. As magnetic activity increases, the size of the oval increases, with the most significant expansion observed on the night side, where it extends both towards the pole and the equator. During major disturbances, the width of the oval can exceed 10° [Starkov, 2000], which can affect magnetic measurements at different latitudes. Regression lines were determined for the indices *PC* (*N*), *AL* , $\sqrt{MPB}$, *ASY* H *H* and *SYM* H *H* in relation to the *SML* -index. The obtained dependencies were close to linear. For the square root of *MPB* we have: $\sqrt{MPB} \approx -0.029 \times SML - 1.09$, for other indices the corresponding expressions are given in [Lyubchich et al., 2023]. The correlation coefficient *R* between $\sqrt{MPB}$ and *SML* equals –0.79. It should be noted that the absolute value of the correlation coefficient is maximum between the indices *AL* and *SML* ($R \approx 0.95$), and minimum between the indices *SYM* H *H* and *SML* $R \approx 0.60$. The closer the absolute value of the correlation coefficient is to one, the closer the dependence is to linear. This result, the proximity of dependencies to linear, is consistent with the power-law, almost quadratic, approximation dependence of the *MPB* index on the indices *PC* (*N*) > 2 (power exponent ~2.4), *SML* (2.3), *ASY* H *H* (2.3) and *SYM* H *H* (2.0). The difference in dynamics of indices *ASY* H *H* and *SYM* H *H* during magnetic storms is discussed in [Dremukhina et al., 2020].

Extremely large values of the interplanetary magnetic field are typically associated with large-scale geoeffective structures of the solar wind - for example, with magnetic clouds or, as in the example in Fig. 1, with the propagation of a coronal mass ejection through the undisturbed solar wind. The impact of such structures on Earth's magnetosphere can cause the development of geomagnetic storms, which, in turn, can lead to the appearance of very large values of the *MPB* -index (see Section 3.1).

The weaker (power-law) dependence of the *MPB* -index on the solar wind dynamic pressure (Fig. 6 *b*) compared to the exponential dependence on its velocity (Fig. 6 *a*), despite the proportionality of the dynamic pressure to the square of the solar wind velocity, can be explained by the fact that statistically the magnitude of the solar wind dynamic pressure increases weakly with increasing velocity. At high solar wind velocity, it typically has low density. For the period of the

11-year solar activity cycle minimum, the weak dependence of dynamic pressure on solar wind velocity was shown, for example, in the work of Lyubchich et al. [2004].

5. CONCLUSIONS

The relationship between the mid-latitude index *MPB* (*Mid-latitude Positive Bays*) with geomagnetic activity and solar wind parameters has been analyzed. The following results were obtained:

– All extremely large values of the *MPB* -index are observed during strong and very strong ($Dst_{min} < -100$ nT) geomagnetic storms. All extremely strong ($Dst_{min} < -250$ nT) geomagnetic storms (superstorms) are accompanied by extremely high values of the *MPB* -index.

– The *MPB* -index statistically increases with increasing geomagnetic activity at any latitude, since there is a correlation between geomagnetic activity at different latitudes.

– The *MPB* -index statistically increases with the growth of both the magnitude of the interplanetary magnetic field and the modulus of any of its components. For the *Bz* -component of the IMF, the dependence on its southern component is stronger.

– The dependence of the *MPB* -index on solar wind speed is more pronounced. The dependence on dynamic pressure and the value of the geoeffective component of the solar wind electric field is also strong. The dependence of the *MPB* -index on solar wind density and temperature is weak.

ACKNOWLEDGMENTS

The authors express their gratitude to the creators of the IMAGE database (http://space.fmi.fi/image/), SuperMAG (http://supermag.jhuapl.edu/) , INTERMAGNET (https://intermagnet.github.io/) for the opportunity to use them in the work. We are grateful to the teams that created and maintain the World Data Center for Geomagnetism, Kyoto (https://wdc.kugi.kyoto-u.ac.jp/) and OMNI (https://cdaweb.gsfc.nasa.gov/) databases and provide free access to the data. We also thank for the opportunity to use *SMU* and *SML* [Newell and Gjerloev, 2011] indices; and collaboration with SuperMAG [Gjerloev et al., 2012].

The authors express their appreciation to Xiangning Chu for kindly providing the opportunity to use the *MPB* -index values.

FUNDING

The work of Despirak Irina Vadimovna and Lyubchich Andris Alekseevich was carried out within the framework of the State assignment of the PGI on the topic "Dynamic processes in the system 'solar wind - magnetosphere - ionosphere' and their influence on the high-latitude ionosphere" (FMES-2022-002).

REFERENCES

– *Werner R., Guineva V., Despirak I.V., Lubchich A.A., Setsko P.V., Atanassov A., Bojilova R., Raykova L., Valev D.* Statistical Studies of Auroral Activity and Perturbations of the Geomagnetic Field at Middle Latitudes // Geomagnetism and Aeronomy. V. 63. N4. P. 473–485. 2023. https://doi.org/10.1134/S0016793223600303

– *Dremukhina L.A., Yermolaev Y.I., Lodkina I.G.* Differences in the dynamics of the asymmetrical part of the magnetic disturbance during the periods of magnetic storms induced by different interplanetary sources // Geomagnetism and Aeronomy. V. 60. N6. P. 714–726. 2020. https://doi.org/10.1134/S0016793220060031

– *Despirak I.V., Kleimenova N.G., Lyubchich A.A., Setsko P.V., Gromova L.I., Werner R.* Global Development of the Supersubstorm of May 28, 2011 // Geomagnetism and Aeronomy. V. 62. №. 3. P. 199 – 208. 2022. https://doi.org/10.1134/S0016793222030069

– *Lyubchich A.A., Despirak I.V., Werner R.* Dependence of the MPB-index on geomagnetic activity and solar wind characteristics // Proc. XLVI Annual Seminar. Apatity. P. 42–47. 2023. https://doi.org/10.51981/2588-0039.2023.46.009

– *Lyubchich A.A., Despirak I.V., Yakhnin A.G.* Correlation between the solar wind pressure and velocity at a minimum of the 11-year cycle // Geomagnetism and Aeronomy. V. 44. N 2. P. 143–148. 2004.

– *Starkov G.V.* Planetary dynamics of auroral luminescence / Physics of near-Earth space. Chapter 3, 4. P. 409–499. Apatity: KSC RAS publishing, 706 p. 2000.

– *Troshichev O.A. PC* -index — a ground-based indicator of incoming solar wind energy to the magnetosphere // Problems of Arctic and Antarctic. №2 (85). P.102–116. 2010.

– *Arnold B.C.* Pareto Distribution / In Wiley StatsRef: Statistics Reference Online (eds N. Balakrishnan, T. Colton, B. Everitt, W. Piegorsch, F. Ruggeri and J.L. Teugels). 2015. https://doi.org/10.1002/9781118445112.stat01100.pub2

– *Chu X* . Configuration and generation of substorm current wedge. Los Angeles: University of California, Los Angeles, 2015. (A dissertation submitted in partial satisfaction of the requirements for the degree Doctor of Philosophy in Geophysics and Space Physics).

– *Coles S.* An Introduction to Statistical Modeling of Extreme Values / Springer, London. 2001.
– *Feldstein Y.I.* Modelling of the magnetic field of magnetospheric ring current as a function of interplanetary medium parameters // Space Sci. Rev. V. 59. P. 83–165. 1992. https://doi.org/10.1007/BF01262538
– *Fu H., Yue C., Zong Q.-G., Zhou X.-Z., Fu S.* Statistical characteristics of substorms with different intensity // J. Geophys. Res.: Space Physics. V. 126. e2021JA029318. 2021. https://doi.org/10.1029/2021JA029318
– *Gonzalez W.D., Echer E., Tsurutani B.T., de Gonzalez A.L.C., Dal Lago A.* Interplanetary origin of intense, superintense and extreme geomagnetic storms // Space Science Reviews. V. 158. N 1. P. 69–89. 2011. https://doi.org/10.1007/s11214-010-9715-2
– *Gonzalez W.D., Tsurutani B.T.* Criteria of interplanetary parameters causing intense magnetic storms (Dst < −100 nT) // Planetary and Space Science. V. 35. N 9. P. 1101–1109. 1987. https://doi.org/10.1016/0032-0633(87)90015-8
– *Gonzalez W.D., Tsurutani B.T., Clúa de Gonzalez A.L.* Interplanetary origin of geomagnetic storms // Space Sci. Rev. V. 88. N 3-4. P. 529–562. 1999. https://doi.org/10.1023/A:1005160129098
– *Gonzalez W.D., Tsurutani B.T., Lepping R.P., Schwenn R.* Interplanetary phenomena associated with very intense geomagnetic storms // Journal of Atmospheric and Solar-Terrestrial Physics. V. 64. N 2. P. 173–181. 2002. https://doi.org/10.1016/S1364-6826(01)00082-7
– *Hajra R., Tsurutani B.T., Echer E., Gonzalez W.D., Gierloev J.W* . Supersubstorms (SML < −2500 nT): Magnetic storm and solar cycle dependences // J. Geophys. Res. V. 121. P. 7805–7816. 2016. https://doi.org/10.1002/2015JA021835
– *Iyemori T., Araki T., Kamei T., Takeda M.* Mid-latitude Geomagnetic Indices "ASY" and "SYM" (Provisional). N3. 1992 // Data Analysis Center for Geomagnetism and Space Magnetism Faculty of Science Kyoto University, ISSN 0918-5763, 1994.
– *Mac-Mahon R.M., Gonzalez W.D.* Energetics during the main phase of geomagnetic superstorm s // J. Geophys. Res. V. 102. A7. P. 14199–14207. 1997. https://doi.org/ 10.1029/97JA01151
– *McPherron L.R., Chu X.* The Mid-Latitude Positive Bay and the MPB Index of Substorm Activity // Space Sci. Rev. V. 206. P. 91–122. 2017. https://doi.org/10.1007/s11214-016-0316-6
– *McPherron L.R., Chu X.* The midlatitude positive bay index and the statistics of substorm occurrence // J. Geophys. Res.: Space Physics. V. 123. N 4. P. 2831–2850. 2018. https://doi.org/10.1002/2017JA024766

– *McPherron R.L., Russell C.T., Aubry M.P.* Satellite studies of magnetospheric substorms on August 15, 1968: 9. Phenomenological model for substorms // J. Geophys. Res. V. 78. N 16. P. 3131–3149. 1973. https://doi.org/10.1029/JA078i016p03131

– *Meng X., Tsurutani B.T., Mannucci A.J.* The Solar and Interplanetary Causes of Superstorms (Minimum Dst ≤ −250 nT) During the Space Age // J. Geophys. Res.: Space Physics. V. 124. N 6. P. 3926 – 3948. 2019. https://doi.org/10.1029/2018JA026425

– *Nakamura M., Yoneda A., Oda M., Tsubouchi K.* Statistical analysis of extreme auroral electrojet indices // Earth, Planets and Space. V. 67. Art. 153. 2015. https://doi.org/10.1186/s40623-015-0321-0

– *Sergeev V.A., Shukhtina M.A., Stepanov N.A., Rogov D.D., Nikolaev A.V., Spanswick E., Donovan E., Raita T., Kero A.* Toward the reconstruction of substorm-related dynamical pattern of the radiowave auroral absorption // Space Weather. V. 18. N 3. e2019SW002385. 2020. https://doi.org/10.1029/2019SW002385

– *Troshichev O.A., Andrezen V.G.* The relationship between interplanetary quantities and magnetic activity in the southern polar cap // Planet. Space Sci. V. 33. N 4. P. 415–419. 1985. https://doi.org/10.1016/0032-0633(85)90086-8

– *Troshichev O.A., Andrezen V.G., Vennerstrøm S., Friis-Christensen E.* Magnetic activity in the polar cap – A new index // Planet. Space Sci. V. 36. N 11. P. 1095–1102. 1988. https://doi.org/10.1016/0032-0633(88)90063-3

– *Tsurutani B.T., Gonzalez W.D., Tang F., Lee Y.T.* Great geomagnetic storms // Geophysical Research Letters. V. 19. N 1. P. 73–76. 1992. https://doi.org/10.1029/91GL02783

– *Tsurutani B.T., Hajra R., Echer E., Gjerloev J.W.* Extremely intense (SML ≤ –2500 nT) substorms: isolated events that are externally triggered? // Annales Geophysicae. V. 33. P. 519–524. 2015. https://doi.org/10.5194/angeo-33-519-2015

– *Tsubouchi K., Omura Y.* Long-term occurrence probabilities of intense geomagnetic storm events // Space Weather. V. 5. N 12. S12003. 2007. https://doi.org/10.1029/2007SW000329

– *Tsyganenko N.A., Andreeva V.A., Sitnov M.I., Stephens G.K., Gjerloev J.W., Chu X., Troshichev O.A.* Reconstructing Substorms via Historical Data Mining: Is It Really Feasible? // J. Geophys. Res.: Space Physics. V. 126. N 10. e2021JA029604 . 2021. https://doi.org/10.1029/2021JA02 9604

– *Wanliss J.A., Showalter K.M.* High-resolution global storm index: *Dst* versus *SYM-H* // J. Geophys. Res. V. 111. N A2. A02202. 2006. https://doi.org/10.1029/2005JA011034

– *Weibull W.* A statistical distribution function of wide applicability // J. Appl. Mech.-Trans. ASME. V. 18. N 3. P. 293–297. 1951. https://doi.org/10.1115/1.4010337

– *Werner R., Guineva V., Atanassov A., Bojilova R., Raykova L., Valev D., Lubchich A., Despirak I.* Calculation of the horizontal power perturbations of the Earth surface magnetic field / Proceedings of the Thirteenth Workshop "Solar Influences on the Magnetosphere, Ionosphere and Atmosphere", September, 2021, Book of Proceedings, https://doi.org/10.31401/WS.2021.proc , p. 159-165.
– *Zong Q.-G., Yue C., Fu S.-Y.* Shock induced strong substorms and super substorms: Preconditions and associated oxygen ion dynamics // Space Sci. Rev. V. 217. N 33. 2021. https://doi.org/10.1007/s11214-021-00806-x

Table 1. List of superstorms recorded from 1991 to 2019 inclusive, ranked by the minimum value of the *Dst* -index.

Dst $_{min}$ **time (dd.mm.yyyy UT)**	***Dst*** $_{min}$ **(nT)**	***SYM-H*** $_{min}$ **/time (nT)/(dd.mm UT)**	***SI*** $^{+}$**/time (nT)/(dd.mm UT)**	**Interplanetary Case**	***MPB*** **/time (nT** ^{2}**)/(dd.mm UT)**
20.11.2003 20:30	–422	–490/20.11 18:17	49/20.11 08:06	Sheath+MC *Bxz* ~69	~69 000/20.11 17:03
31.03.2001 08:30	–387	–437/31.03 08:06	129/31.03 01:00	Sheath+MC *Bxzc* ~26	~26 000/31.03 06:09 ~21 000/31.03 15:53
30.10.2003 22:30	–383	–432/30.10 22:55	76/30.10 20:08	Sheath	~46 000/30.10 21:35
08.11.2004 06:30	–374	–394/08.11 05:55	92/07.11 19:20	Sheath+MC *Bxz* ~27	~27 000/08.11 01:19 [MPB X~9 300]
09.11.1991 01:30	–354	–402/09.11 01:32	49/08.11 13:15	Unknown	~575 000/08.11 22:20
30.10.2003 00:30	–353	–391/30.10 01:48	81/29.10 06:14	Sheath+MC *Bxz* ~69	~69 000/29.10 19:56
16.07.2000 00:30	–301	–347/15.07 21:54	93/15.07 15:04	MC *Bxz* ~23	~23 000/15.07 21:48
25.03.1991 00:30	–298	–337/25.03 03:41	118/24.03 03:55	Unknown	~105 000/24.03 21:33 ~24 000/24.03 04:06
06.11.2001 00:30	–292	–320/06.11 04:06	88/06.11 01:54	PICME+sheath	~11 000/06.11 02:05 [MPB X~6 300]
10.05.1992 14:30	–288	–363/10.05 14:15	81/09.05 20:02	Likely sheath+MC	~28 000/10.05 18:29
07.04.2000 00:30	–288	–320/07.04 00:09	46/06.04 16:45	Sheath	~60 000/06.04 23:27
11.04.2001 23:30	–271	–280/11.04 23:57	26/11.04 15:53	Sheath	~24 000/11.04 21:37 ~23 000/12.04 00:16
10.11.2004 10:30	–263	–282/10.11 09:31	46/09.11 18:51	Sheath+MC *Bxz* +	~31 000/09.11 20:32
29.10.1991 07:30	–254	–284/29.10 08:02	51/28.10 11:03	Sheath+MC *Bxz* +	~223 000/28.10 16:06

Note: The first five columns are taken from Table 1 in the article by Meng et al. [2019]. They sequentially show the registration time of *Dst* $_{min}$ (1); its value (2); the value and registration time of *SYM* H H_{min} (3); the value and registration time of the sudden impulse *SI* $^{+}$ (4); the structure in the

solar wind that caused the magnetic storm (5). The last column shows the value and registration time of the extreme value of the *MPB* -index (6).

Table 2. Strong storms, ranked by Dst_{min}, during which extremely large values of *MPB* -index were observed.

Dst_{min} **time** (dd.mm.yyyy UT)	Dst_{min} (nT)	*SYM* H H_{min} /time (nT)/(dd.mm UT)	*MPB* /time (nT^2)/(dd.mm UT)
15.05.2005 08:30	–247	–305/15.05 08:20	~38 000/15.05 08:50
05.06.1991 19:30	–223	–238/05.06 16:56	~50 000/05.06 17:14
24.11.2001 16:30	–221	–234/24.11 12:37	~49 000/24.11 07:15
01.11.1991 23:30	–196	–200/01.11 19:37 20:22	~36 000/01.11 20:30
13.07.1991 15:30	–183	–238/13.07 15:42	~42 000/13.07 16:20
01.10.2002 16:30	–176	–154/01.10 12:53	~18 000/01.10 16:28
26.08.2018 06:30	–175	–206/26.08 07:11	~18 000/26.08 07:44
26.02.1992 22:00	–174	–167/26.02 22:31	~61 000/26.02 19:44
08.02.1992 16:30	–114	–126/08.02 15:18	~41 000/08.02 15:35

Note: The columns sequentially show the time of registration Dst_{min} (1); its value (2); the value and time of registration of *SYM* H H_{min} (3); the value and time of registration of the extreme value of the *MPB* -index (4).

Figure captions

Fig. 1. Example of observation of extremely large values of the *MPB* -index during the day starting from 12:00 UT on 06.04.2000. From top to bottom, the behavior of the IMF modulus, *By and иBz components* of the IMF in the coordinate system *GSM* , the velocity, density, temperature and dynamic pressure of the solar wind, as well as geomagnetic indices *PC* (*N*), *SYM* H *H* and *Dst* , *AL* and *SML* , *MPB* .

Fig. 2. Distribution *MPB* -index by values, plotted on a double logarithmic scale. Step on the horizontal axis is 1 nT^2. The wide gray line shows the linear approximation of the distribution tail (above 200 nT^2) in a bilogarithmic coordinate system.

Fig. 3. Distribution of *SML* -index by values on a double logarithmic scale (left), regression lines *MPB* (*SML*) (in the center) and *SML* (*MPB*) (right). Gray lines show approximation dependencies.

Fig. 4. Distribution of indices by values (top) and their relationship with the *MPB* index (bottom). On the left (*a*) for the *PC* (*N*) index, in the center (*b*) for the *ASY* H *H* index and on the right (*c*) for the *SYM* H *H* index. Wide gray lines show approximation dependencies.

Fig. 5. Dependence of the *MPB* -index on the IMF magnitude (left) and on *By* (center) and *Bz* (right) components of the IMF in the *GSM* coordinate system.

Fig. 6. Dependence of the *MPB* -index: (*a*) on the V_X-component of the SW velocity, (*b*) on the dynamic pressure of the SW and (*c*) on the geoeffective component of the electric field $E_{Y\,GSM}$ of the solar wind. Gray lines show approximation dependencies.

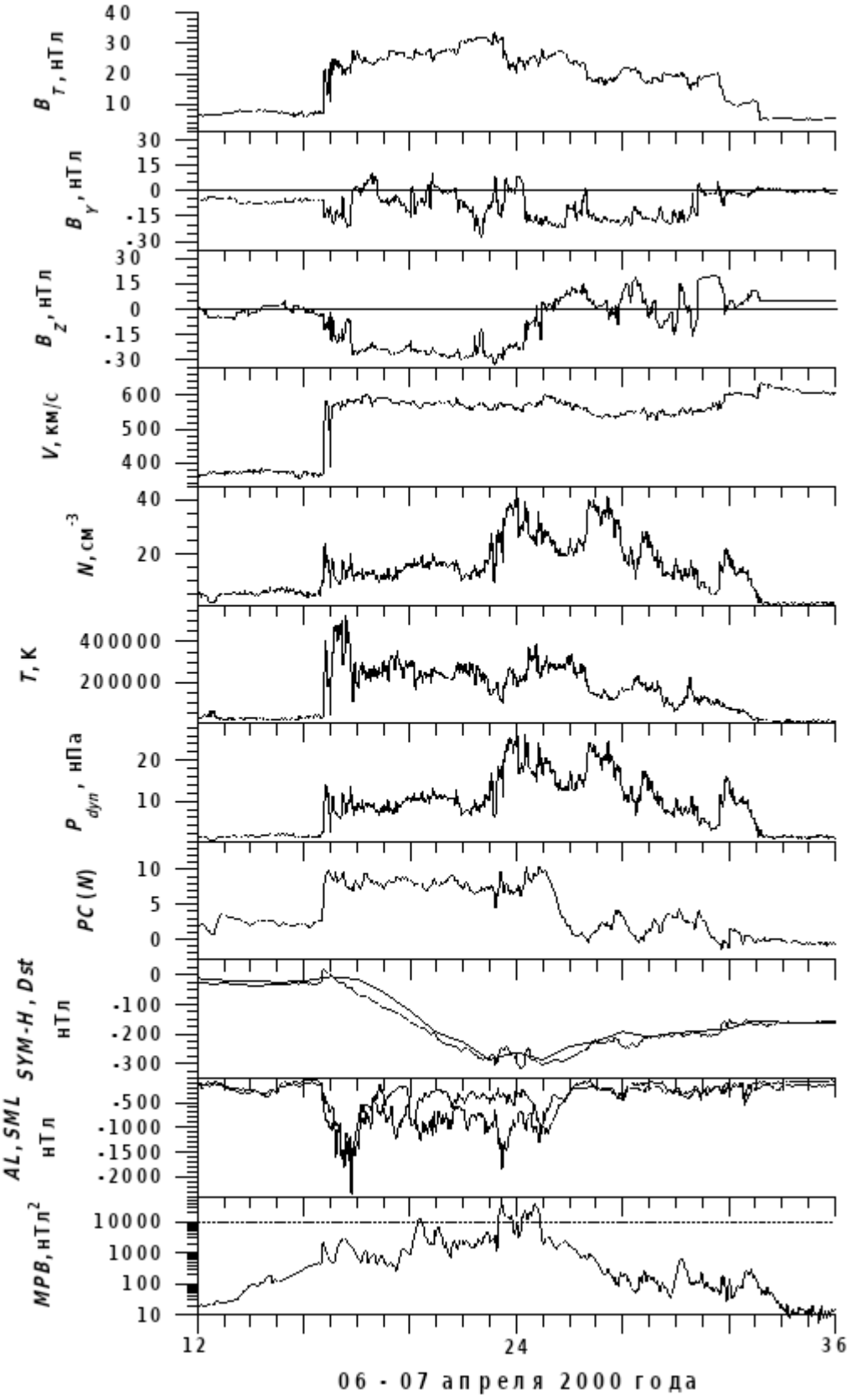
B_T, нТл
40
30
20
10
B_y, нТл
30
15
0
-15
-30
B_Z, нТл
30
15
0
-15
-30
V, км/с
600
500
400
N, см$^{-3}$
40
20
T, K
400000
200000
P_{dyn}, нПа
20
10
$PC(N)$
10
5
0
SYM-H, Dst
нТл
0
-100
-200
-300
AL, SML
нТл
-500
-1000
-1500
-2000
MPB, нТл^2
10000
1000
100
10
12
24
36
06 - 07 апреля 2000 года

Fig. 1

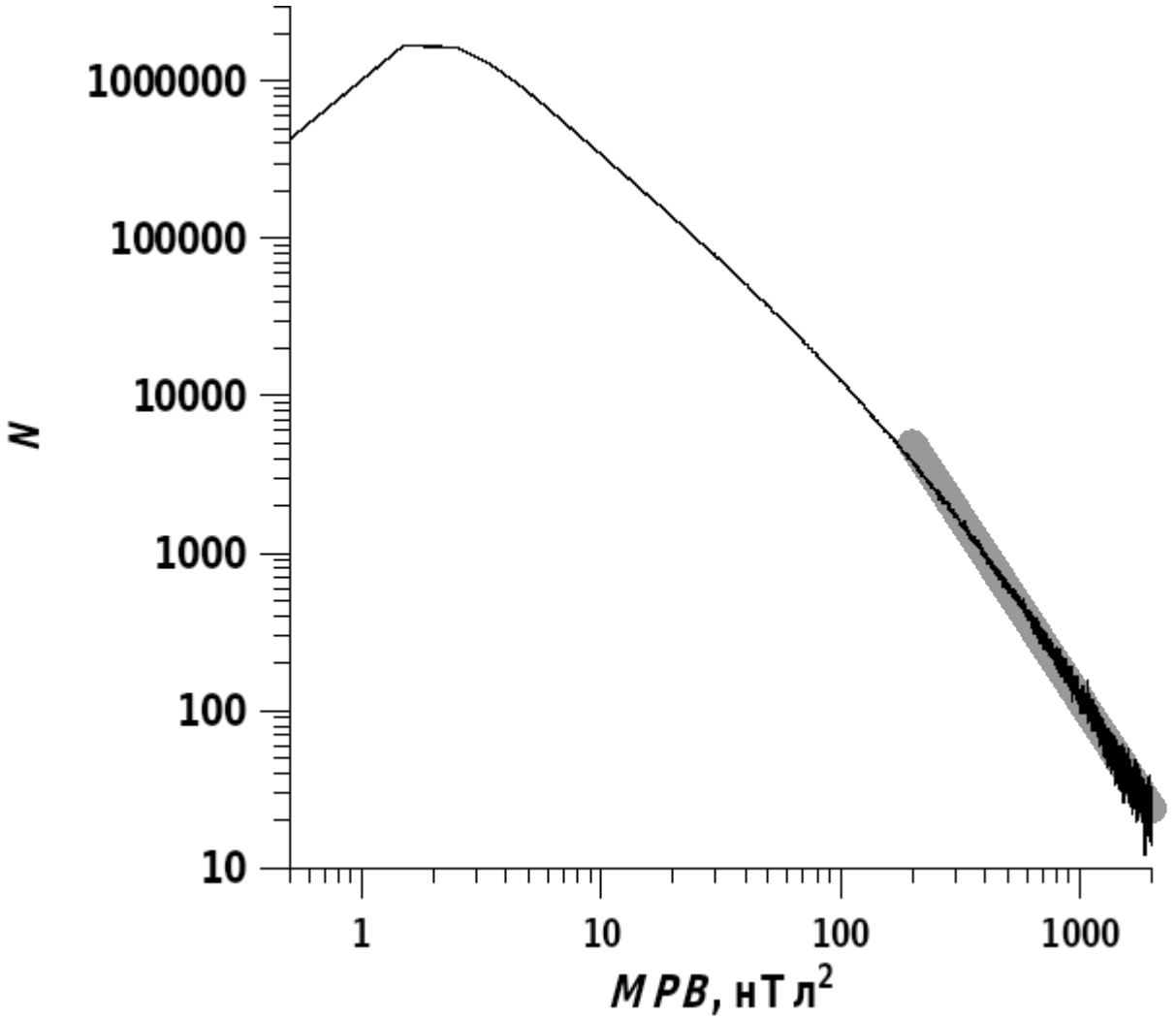
1000000
100000
10000
1000
100
10
N
1
10
100
1000
MPB, нТл²

Fig. 2

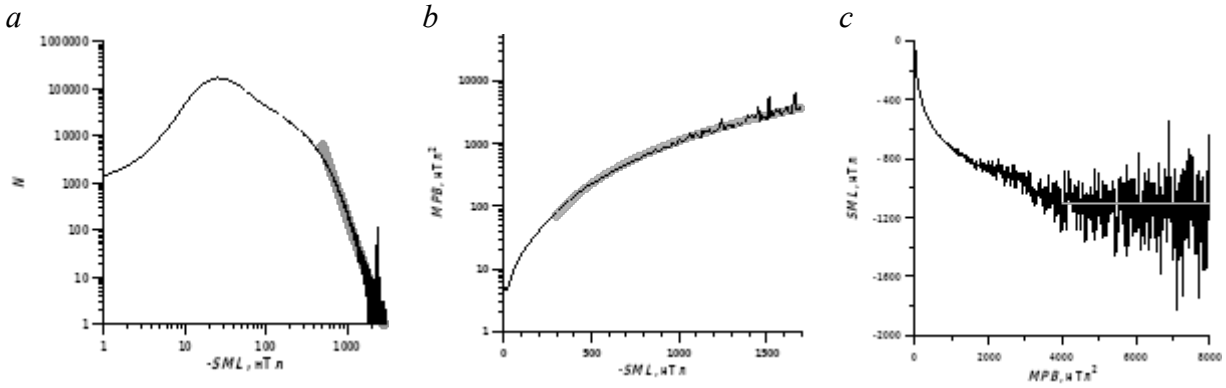
a
b
c
N
-SML, нТл
MPB, нТл²
SML, нТл

Fig. 3

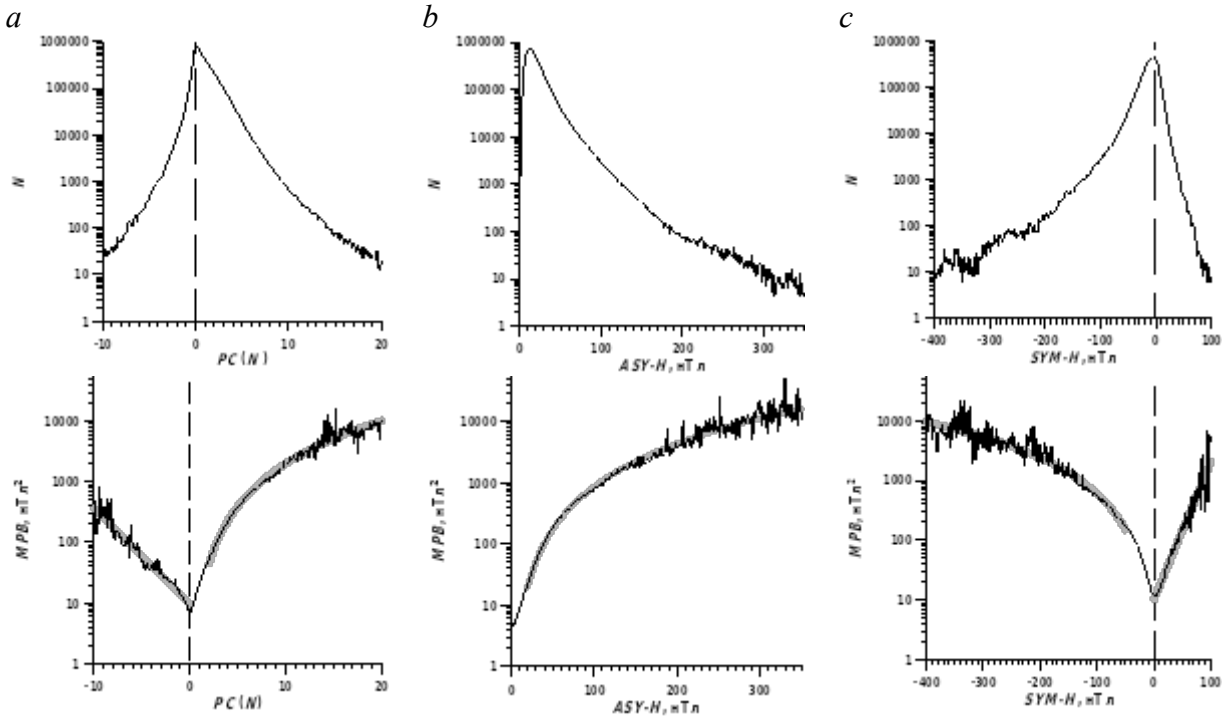

Fig. 4

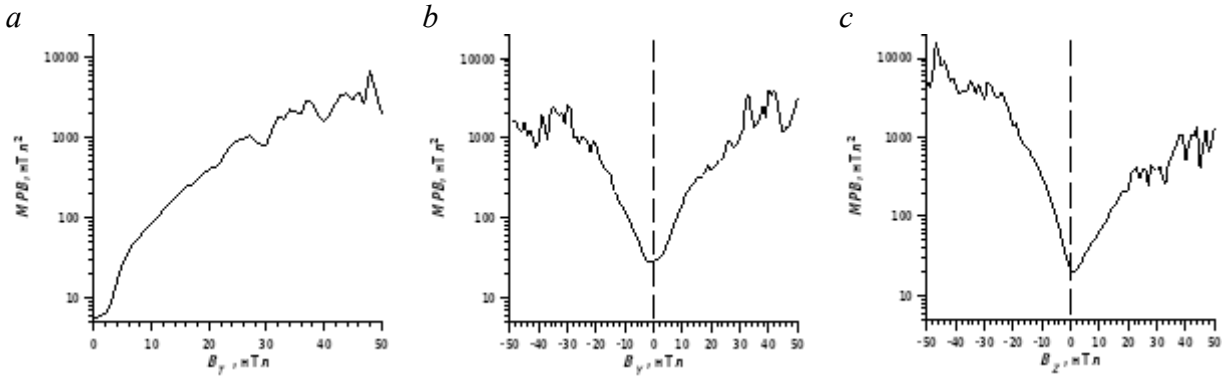

Fig. 5

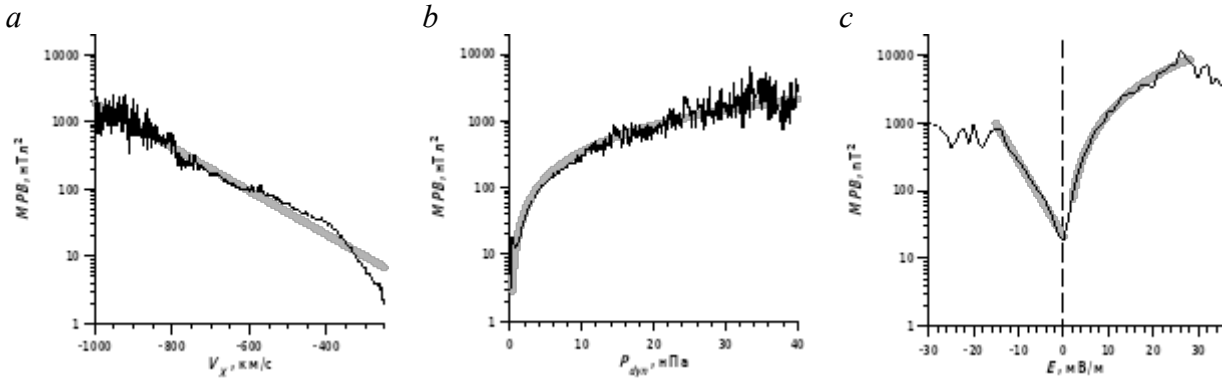
a
b
c
MPB, нТл²
10000
1000
100
10
1
-1000
-800
-600
-400
V_x, км/с
0
10
20
30
40
$P_{дин}$, нПа
-30
-20
-10
0
10
20
30
E, мВ/м

Fig. 6